1	
2	Quantification and evaluation of atmospheric pollutant
3	emissions from open biomass burning with multiple methods:
4	A case study for Yangtze River Delta region, China
5	
6	Yang Yang ¹ and Yu Zhao ^{1,2*}
7	
8 9	1. State Key Laboratory of Pollution Control & Resource Reuse and School of the Environment, Nanjing University, 163 Xianlin Ave., Nanjing, Jiangsu 210023, China
10 11 12 13	2. Jiangsu Collaborative Innovation Center of Atmospheric Environment and Equipment Technology (CICAEET), Nanjing University of Information Science & Technology, Jiangsu 210044, China
14	
15	*Corresponding author: Yu Zhao
16	Phone: 86-25-89680650; email: <u>yuzhao@nju.edu.cn</u>

18

Abstract

19 Air pollutant emissions from open biomass burning (OBB) in Yangtze River Delta (YRD) were estimated for 2005-2015 using three (traditional bottom-up, fire 20 radiative power (FRP)-based, and constraining) approaches, and the differences 21 between those methods and their sources were analyzed. The species included PM_{10} , 22 PM_{2.5}, organic carbon (OC), elemental carbon (EC), CH₄, non-methane volatile 23 organic compounds (NMVOCs), CO, CO₂, NO_x, SO₂ and NH₃. The inter-annual 24 trends in emissions with FRP-based and constraining methods were similar with the 25 fire counts in 2005-2012, while that with traditional method was not. For most years, 26 emissions of all species estimated with constraining method were smaller than those 27 with traditional method except for NMVOCs, while they were larger than those with 28 FRP-based except for EC, CH₄ and NH₃. Such discrepancies result mainly from 29 different masses of crop residues burned in the field (CRBF) estimated in the three 30 31 methods. Chemistry transport modeling (CTM) was applied using the three OBB 32 inventories. The simulated PM₁₀ concentrations with constrained emissions were closest to available observations, implying constraining method provided the best 33 emission estimates. CO emissions in the three methods were compared with other 34 studies. Similar temporal variations were found for the constrained emissions, 35 36 FRP-based emissions, GFASv1.0 and GFEDv4.1s, with the largest and the lowest emissions estimated for 2012 and 2006, respectively. The temporal variations of the 37 emissions based on traditional method, GFEDv3.0 and Xia et al. (2016) were different 38 with them. The constrained CO emissions in this study were commonly smaller than 39 those based on traditional bottom-up method and larger than those based on burned 40 area or FRP in other studies. In particular, the constrained emissions were close to 41 GFEDv4.1s that contained emissions from small fires. The contributions of OBB to 42 two particulate pollution events in 2010 and 2012 were analyzed with brute-force 43 method. Attributed to varied OBB emissions and meteorology, the average 44 contribution of OBB to PM₁₀ concentrations in June 8-14 2012 was estimated at 45 37.6% (56.7 µg/m³), larger than that in June 17-24, 2010 at 21.8 % (24.0 µg/m³). 46 Influences of diurnal curves of OBB emissions and meteorology on air pollution 47 caused by OBB were evaluated by designing simulation scenarios, and the results 48 suggested that air pollution caused by OBB would become heavier if the 49 meteorological conditions were unfavorable, and that more attention should be paid to 50

the OBB control at night. Quantified with Monte-Carlo simulation, the uncertainty of traditional bottom-up inventory was smaller than that of FRP-based one. The percentages of CRBF and emission factors were the main source of uncertainty for the two approaches, respectively. Further improvement on CTM for OBB events would help better constraining OBB emissions.

- 56
- 57

1. Introduction

Open biomass burning (OBB) is an important source of atmospheric particulate 58 matter (PM) and trace gases including methane (CH₄), non-methane volatile organic 59 60 compounds (NMVOCs), carbon monoxide (CO), carbon dioxide (CO₂), oxides of nitrogen (NO_X), sulfur dioxide (SO₂), and ammonia (NH₃) (Andreae and Merlet, 2001; 61 62 van der Werf et al., 2010; Wiedinmyer et al., 2011; Kaiser et al., 2012; Giglio et al., 2013, Qiu et al., 2016; Zhou et al., 2017a). As it has significant impacts on air quality 63 and climate (Crutzen and Andreae, 1990; Cheng et al., 2014; Hodzic and Duvel, 2018), 64 it is important to understand the amount, temporal variation and spatial pattern of 65 66 **OBB** emissions.

Various methods have been used to estimate OBB emissions, including 67 traditional bottom-up method that relied on surveyed amount of biomass burning 68 69 (traditional bottom-up method), the method based on burned area or fire radiative power (BA or FRP method), and emission constraining with chemistry transport 70 model (CTM) and observation (constraining method). In the traditional bottom-up 71 method that was most frequently used, emissions were calculated as a product of crop 72 production level, the ratio of straw to grain, percentage of dry matter burned in fields, 73 74 combustion efficiency, and emission factor (Streets et al., 2003; Cao et al., 2007; Wang and Zhang, 2008; Zhao et al., 2012; Xia et al., 2016, Zhou et al., 2017a). The 75 BA or FRP method was developed along with progress of satellite observation 76 technology. BA was detected through remote sensing, and used in OBB emission 77 calculation combined with ground biomass density burned in fields, combustion 78 79 efficiency and emission factor. As burned area of each agricultural fire was usually small and difficult to be detected, this method could seriously underestimate the 80 81 emissions (van der Werf et al., 2010; Liu et al., 2015). In FRP-based method, fire radiative energy (FRE) was calculated with FRP at over pass time of satellite and the 82 83 diurnal cycle of FRP. The mass of crop residues burned in the field (CRBF) were then

obtained based on combustion conversion ratio and FRE, and emissions were 84 calculated as a product of the mass of CRBF and emission factor (Kaiser et al., 2012; 85 Liu et al., 2015). In the constraining method, observed concentrations of atmospheric 86 compositions were used to constrain OBB emissions with CTM (Hooghiemstra et al., 87 2012; Krol et al., 2013; Konovalov et al., 2014). The spatial and temporal 88 distributions of OBB emissions were derived from information of fire points from 89 satellite observation. Although varied methods and data sources might lead to 90 discrepancies in OBB emission estimation, those discrepancies and underlying 91 92 reasons have seldom been thoroughly analyzed in previous studies. Moreover, few studies applied CTM to evaluate emissions obtained from different methods, thus the 93 uncertainty and reliability in OBB emission estimates remained unclear. 94

Due to growth of economy and farmers' income, a large number of crop straws 95 were discharged and burned in field, and OBB (which refers to crop straws burned in 96 fields in this paper) became an important source of air pollutants in China (Streets et 97 al., 2003; Shi and Yamaguchi 2014; Qiu et al., 2016; Zhou et al., 2017a). It brings 98 additional pressure to the country, which is suffering poor air quality (Richter et al., 99 2005; van Donkelaar et al., 2010; Xing et al., 2015; Guo et al., 2017) and making 100 101 efforts to reduce pollution (Xia et al., 2016; Zheng et al., 2017). Located in the eastern China, Yangtze River Delta (YRD) including the city of Shanghai and the provinces 102 103 of Anhui, Jiangsu and Zhejiang is one of China's most developed and heavy-polluted regions (Ran et al., 2009; Xiao et al., 2011; Cheng et al., 2013, Guo et al., 2017). 104 105 Besides intensive industry and fossil fuel combustion, YRD is also an important area of agriculture production, and frequent OBB events aggravated air pollution in the 106 region (Cheng et al., 2014). 107

In this study, we chose YRD to develop and evaluate high resolution emission 108 inventories of OBB with different methods. Firstly, we established YRD's OBB 109 emission inventories for 2005-2012 using the traditional bottom-up method (the 110 percentages of CRBF for 2013-2015 were currently unavailable), and inventories for 111 2005-2015 using FRP-based and constraining methods. The three inventories were 112 then compared with each other and other available studies, in order to discover the 113 differences and their origins. Meanwhile, the three inventories were evaluated using 114 Models-3 Community Multi-scale Air Quality (CMAQ) system and available ground 115 observations. Contributions of OBB to particulate pollution during three typical OBB 116 events in 2010, 2012 and 2014 were evaluated through brute-force method. Influences 117

of meteorology and diurnal curves of OBB emissions on air pollution caused by OBB
were also analyzed by designing simulation scenarios. Finally, uncertainties of the
three OBB inventories were analyzed and quantified with Monte-Carlo simulation.

- 121
- 122

2. Data and methods

123

2.1 Traditional bottom-up method

Annual OBB emissions in YRD were calculated by city from 2005 to 2012 usingthe traditional bottom-up method with following equations:

126
$$E_{(i,y),j} = \sum_{k} \left(M_{(i,y),k} \times EF_{j,k} \right)$$
 (1)

127
$$M_{(i,y),k} = P_{(i,y),k} \times R_k \times F_{(i,y)} \times CE_k$$
(2)

where *i* and y indicate city and year (2005-2012), respectively; *j* and *k* represent species and crop type, respectively; *E* is the emissions, metric ton (t); *M* is the mass of CRBF, Gg; *EF* is the emission factor, g/kg; *P* is the crop production, Gg; *R* is the ratio of grain to straw (dry matter); *F* is the percentage of CRBF; and *CE* is the combustion efficiency.

As summarized in Table S1 in the supplement, emission factors were obtained 133 based on a comprehensive literature review, and those developed in China were 134 selected preferentially. The mean value was used if various emission factors could be 135 obtained. When the emission factors for one crop straw were not obtained, the mean 136 value of the others was used instead. Annual production of crops at city level was 137 taken from statistical yearbooks (NBS, 2013). The ratios of straw to grain for different 138 crops were obtained from Bi (2010) and Zhang et al. (2008), and the combustion 139 efficiencies for different crop were obtained from Wang et al. (2013), as provided in 140 Table S2 in the supplement. Without officially reported data, the percentages of CRBF 141 were estimated to be half of the percentages of unused crop residues, following Su et 142 al. (2012). In Jiangsu, the percentages of unused crop residues were officially reported 143 for 2008, 2011 and 2012, while data for other years were unavailable. In this work, 144 therefore, the percentages of CRBF were assumed to be constant before 2008 and to 145 146 decrease by same rate (-15.2%) from 2008 to 2011, since a provincial plan was made in 2009 to increase the utilization of straw (JPDRC and SMAC, 2009). Similarly, the 147 percentages of CRBF for Shanghai were assumed to be constant before 2008 and to 148 decrease by same rate (-16.8%) from 2008 to 2012. Without any official plans 149

released, in contrast, constant percentages of CRBF were assumed for Zhejiang and Anhui before 2011, and that for 2012 was taken from NDRC (2014). We applied uniform percentages of CRBF for cities within a province attributed to lack of detailed information at city level, as summarized in Table S3 in the supplement. OBB emissions after 2012 were not calculated with the traditional bottom-up method, attributed to lack of information on percentages of CRBF and unused crop residues for corresponding years.

157 2.2 FRP-based method

Similar to traditional bottom-up method, OBB emissions of FRP-based method were calculated by multiplying the mass of CRBF and emission factors of various pollutants, but mass of CRBF were derived from FRP instead of government-reported data. As the burned crop types could not be identified with FRP, uniform emission factors were applied for different crop types (Randerson et al., 2018; Liu et al., 2016; Qiu et al., 2016), as provided in Table S4 in the supplement.

164 165 The mass of CRBF was calculated with the following equation: $M = FRE \times CR$

(3)

where *M* represents the mass of CRBF, kg; *CR* represents the combustion conversion 166 ratio from energy to mass (kg/MJ); and FRE represents the total released radiative 167 energy in an active fire pixel obtained from satellite observation (MJ). We used a 168 169 combustion ratio (CR) of 0.41 ± 0.04 (kg/MJ) based on the results of Wooster et al. 170 (2005) in the field and Freeborn et al. (2008) in the laboratory. Diurnal cycle of FRP from crop burning was assumed to follow a Gaussian distribution. Following Vermote 171 et al. (2009) and Liu et al. (2015), FRE was calculated using a modified Gaussian 172 function as below: 173

174
$$FRE = \int FRP = \int_{0}^{24} FRP_{\text{peak}} \left(b + e^{-\frac{(t-h)^2}{2\sigma^2}} \right) dt$$
(4)

175
$$FRE_{\text{peak}} = \frac{FRP_t}{\left[b + e^{\frac{(t-b)^2}{2\sigma^2}}\right]}$$
(5)

where FRP_{peak} is the peak fire radiative power in the fire diurnal cycle; *t* is the overpass time of satellite; and *b*, σ , and *h* represent the background level of the diurnal cycle, the width of fire diurnal curve, and the peak hour (local time, LT), respectively.

FRP data were taken from MODIS Global Monthly Fire Location Product(MCD14ML) which provides data from both the Terra and Aqua satellites (Davies et

al., 2009). The active fire data in MCD14ML were derived from Terra with overpass 181 times at approximately 10:30 AM and 10:30 PM LT and Aqua satellite with overpass 182 times at 1:30 AM and 1:30 PM LT. The fire products provided the geographic 183 coordinates of fire pixels (also known as fire points), overpass times, satellites and 184 their FRP values. The land cover dataset (GlobCover2009) was used to define 185 186 croplands (European Space Agency and Université Catholique de Louvain, 2011).

Parameters b, σ , and h from 2005 to 2015 were calculated using the inter-annual 187 Terra to Aqua (T/A) FRP ratios provided in Table S5 in the supplement: 188

189
$$b = 0.86r^2 - 0.52r + 0.08$$
 (6)
190

191
$$\sigma = 3.89r + 1.03$$
 (7)

193
$$h = -1.23r + 14.57 + \varepsilon$$
 (8)

where r represents the average T/A FRP ratio. Following Liu et al. (2015), we added a 194 parameter ε (4h) to modify FRP_{peak} hour (h) of the diurnal curve, and the modified 195 FRP diurnal curves could better represent observed FRP temporal variability than the 196 197 original, as shown in Figure S1 in the supplement. As a result, FRE was calculated to range from 1.49×10^6 MJ in 2009 to 1.95×10^6 MJ in 2005, with a mean value of 198 1.74×10^{6} MJ for YRD region (Table S5). 199

To further understand the sources of discrepancies between bottom-up and 200 FRP-based methods, the emission factors applied in the bottom-up method were 201 202 weighted with the masses of various crop types and used to estimate the OBB emissions for 2010 with the FRP-based method. The estimated OBB emissions 203 204 (FRP-based (WSE)) were compared with the emissions based on bottom-up method in 205 section 3.3.

206

192

2.3 Constraining method

CTM and observation of ground particle matter (PM) concentrations were 207 applied in constraining OBB emissions given the potentially big contribution of OBB 208 to particle pollution for harvest seasons (Fu et al., 2013; Cheng et al., 2014; Li et al., 209 2014). To characterize the non-linearity between emissions and concentrations, an 210 initial inventory including OBB and other sources was applied in CTM, and the 211 response of PM concentrations to emissions was calculated by changing OBB 212 emissions by a certain fraction (5% in this study) in the model. We defined a response 213 coefficient as the ratio of relative change in PM concentrations to that in OBB 214

emissions. Simulated PM concentrations were then compared with available 215 observation, and the mass of CRBF and OBB emissions of all species were corrected 216 combining the obtained response coefficient and the discrepancy between observed 217 and simulated PM concentrations. The corrected emissions were further applied in 218 CTM and the process (including recalculation of response coefficient) repeated until 219 220 the discrepancies between observation and simulation was small enough (the value of I in equation (9) is less than 0.1% in this study). To limit the potential uncertainty in 221 emissions from other sources, the differences between simulated and observed PM 222 223 concentrations for non-OBB event period were included in the analysis:

224
$$I = \frac{\left| \sum_{x,i} S_{x,i} - \sum_{x,i} Q_{x,i} \times N_i \right|}{\sum_{x,i} O_{x,i}} - 1$$
(9)

where x and i stand for the time (time interval of simulation is hour) and city, respectively; O is the observed PM concentration; S and Q are the simulated PM concentration with and without OBB emissions, respectively; and N is the normalized mean bias (NMB) for non-OBB event period.

229 As primary particles emitted from OBB are almost fine ones, ambient PM_{2.5} concentrations were commonly observed to account for large fractions of PM₁₀ during 230 the OBB event. Figure S2 shows the observed concentrations of $PM_{2.5}$ and PM_{10} at 231 Caochangmen station in Nanjing (the capital of Jiangsu) in June 2012, and the 232 233 average mass ratio of PM_{2.5} to PM₁₀ reached 79% during the OBB event in June 8-14, 2012. The ratios might be even higher in northern YRD where most fire points were 234 235 detected. As ground PM_{2.5} concentrations were unavailable in most cities of northern YRD before 2013, we expected that PM₁₀ was an appropriate indicator for OBB 236 pollution, and observed PM₁₀ concentrations were used to constrain OBB emissions 237 instead in this study. The daily mean PM₁₀ concentrations of all cities were derived 238 from the officially reported Air Pollution Index (API) by China National 239 Environmental Monitoring Center (http://www.cnemc.cn/). The conversion from API 240 scores to PM₁₀ concentrations is discussed in the Supplement. 241

Figure 1 illustrated the spatial patterns of fire points (panels a1 and a2) in June 243 2010 and 2012, city-level PM_{10} concentrations in YRD region in June 2010 and 2012 244 (panels b1 and b2), and temporal variations of daily fire occurrences in June 2010 and 245 2012 (panels c1 and c2). From 2005 to 2012, most OBB activities were found in June

2010 and 2012 and northern YRD was the region with the intensive fire counts. 246 Accordingly PM₁₀ concentrations in northern YRD cities were higher than those in 247 more developed and industrialized cities in the eastern YRD (e.g., Shanghai, Suzhou, 248 Wuxi, and Changzhou), because emissions of OBB overwhelmed those from other 249 sources (Li et al., 2014; Huang et al., 2016). Therefore we constrained OBB emissions 250 with observed PM₁₀ concentrations in northern YRD cities including Xuzhou, 251 Lianyungang, Fuyang, Bengbu, Huainan, Hefei, Chuzhou and Bozhou. Suggested by 252 the monthly and daily distribution of fire counts (Figures S3 and 1c), two strong OBB 253 254 events were defined for June 17-24, 2010 and June 8-14, 2012, and other days in June of 2010 and 2012 were defined as non-OBB event period. For other years, OBB 255 emissions were first scaled from the constrained emissions in 2010 and 2012 with the 256 ratios of FRE for corresponding year to that for 2010 and 2012 respectively, and then 257 calculated as average of the two. Remarkably, the correction of activity level was 258 based on the comparisons of simulated and observed PM₁₀ concentrations, and the 259 emissions of other species were revised according to the changed activity level. The 260 reliability of emission estimation for other species thus depended largely on the 261 reliability of emission factors for PM₁₀ and those species. Uncertainty would be 262 263 introduced to the method, attributed to lack of sufficient and qualified domestic measurements on emission factors. 264

Traditional bottom-up method was used to calculate the initial emission input for all species (NMVOCs emission factor was taken from FRP-based method instead as those in bottom-up method (Li et al., 2007) did not contain oxygenated VOCs). In contrast to application of uniform percentage of CRBF within one province, however, percentage of CRBF for each city was calculated based on that in whole YRD and the fraction of FRP in the city to total YRD FRP, to make the spatial distribution of OBB emissions consistent with that of FRP all over YRD region:

272
$$F_{(i,y)} = \frac{FRP_{(i,y)}}{FRP_{(YRD,y)}} \times \frac{\sum_{k}^{k} P_{(YRD,y),k}}{\sum_{k}^{k} P_{(i,y),k}} \times F_{(YRD,y)}$$
(10)

where *i* and *k* represent city and crop type, respectively; *y* indicates the year (2010 and 2012); *F*, *P*, and *FRP* are the percentage of CRBF, crop production, and fire radiative power, respectively. The initial percentage of CRBF for total YRD ($F_{(YRD,y)}$ in eq (10)) was expected to have limited impact on the result and it was set at 10%, smaller than those in previous studies (Streets et al., 2003; Cao et al., 2007; Wang and Zhang, 2008;
Zhao et al., 2012; Xia et al., 2016, Zhou et al., 2017a).

279 2.4 Temporal and spatial distributions

The spatial and temporal patterns of OBB emissions in the three inventories were determined according to the FRP of agricultural fire points. The emissions of *m*-th grid in region u on *n*-th day in year y were calculated using equation (11):

283
$$E_{(m,n),j} = \frac{FRP_{(m,n)}}{FRP_{(u,y)}} \times E_{(u,y),j}$$
(11)

where $FRP_{(m,n)}$ is the FRP of *m*-th grid on *n*-th day; $FRP_{(u,y)}$ and $E_{(u,y),j}$ are the total FRP and OBB emissions of species *j* for region *u* in year y, respectively. The region *u* indicates city for FRP-based and constraining method, while it indicates province for traditional bottom-up method since uniform percentages of CRBF was applied within the same province in the method.

289 2.5 Configuration of air quality modeling

The Models-3 Community Multi-scale Air Quality (CMAQ) version 4.7.1 was 290 applied to constrain OBB emissions and to evaluate OBB inventories with different 291 methods. As shown in Figure 2, one-way nested domain modeling was conducted, and 292 the spatial resolutions of the two domains were set at 27 and 9 km respectively in 293 Lambert Conformal Conic projection, centered at (110°E, 34°N) with two true 294 latitudes 25 and 40° N. The mother domain (D1, 180×130 cells) covered most parts 295 of China, Japan, North and South Korea, while the second domain (D2, 118×97 cells) 296 covered the whole YRD region. OBB inventories developed in this work were applied 297 in D2. Emissions from other anthropogenic sources in D1 and D2 were obtained from 298 the downscaled the Multi resolution Emission Inventory for China (MEIC, 299 http://www.meicmodel.org/) with an original spatial resolution of 0.25°×0.25°. 300 Population density was applied to relocate MEIC to each modeling domain. Biogenic 301 302 emission inventory was from the Model Emissions of Gases and Aerosols from Nature developed under the Monitoring Atmospheric Composition and Climate 303 project (MEGAN MACC, Sindelarova et al., 2014), and the emission inventories of 304 Cl, HCl and lightning NO_x were from the Global Emissions Initiative (GEIA, Price et 305 al., 1997). Meteorological fields were provided by the Weather Research and 306 Forecasting Model (WRF) version 3.4, and the carbon bond gas-phase mechanism 307

308 (CB05) and AERO5 aerosol module were adopted. Other details on model
309 configuration and parameters were given in Zhou et al. (2017b).

Meteorological parameters of WRF model were compared with the observation 310 dataset of US National Climate Data Center (NCDC), as summarized in Table S6 in 311 the Supplement. For June 2010, the average biases between the two datasets were 312 0.06 m/s for wind speed, 9.84 degree for wind direction, 0.64 K for temperature and 313 2.99% for relative humidity. The analogue numbers were 0.01 and 0.67 m/s, 7 and 314 18.22 degree, 0.91 and 0.43 K and 3.1 and 0.07% respectively for June 2012 and 2014, 315 316 respectively. The meteorological parameters of this study were in compliance with the benchmarks derived from Emery et al. (2001) and Jiménez et al. (2006). Simulated 317 daily PM₁₀ concentrations were compared with observation for non-OBB event period 318 in June 2010 and 2012 in Table S7 in the supplement. The average of normalized 319 mean biases (NMB) and normalized mean errors (NME) were -19.2% and 38.9% for 320 17 YRD cities in June 2010, and -20.9% and 33.9% for 22 cities in June 2012, 321 respectively. Simulated daily and hourly PM₁₀ and PM_{2.5} concentrations were 322 compared with the observation for non-OBB event period in June 2014 in Table S8 in 323 the supplement. The hourly NMB of PM_{2.5} and PM₁₀ were -29.9% and -39.8%, and 324 325 the hourly NME of PM_{2.5} and PM₁₀ were 49.8% and 54.7%. The model performance was similar with that derived by Zhang et al. (2006) in US in general. As shown in 326 327 Figure S4 in the supplement, moreover, simulated hourly PM₁₀ and PM_{2.5} concentrations were in good agreement with observations at four air quality 328 329 monitoring sites in YRD during non-OBB event period in June 2012. The comparison thus implied the reliability of emission inventory of anthropogenic origin used in this 330 work, while underestimation might occur indicated by the negative NMB. 331

332

333

3. Results and discussions

334 3.1 OBB emissions estimated with the three methods

OBB emissions estimated with the traditional bottom-up method for 2005-2012 were shown in Table S9 in the supplement. As emission factors were assumed unchanged during the period, similar inter-annual trends were found for all species and CO_2 was selected as a representative species for further discussion. As shown in Figure 3, CO_2 emissions from traditional bottom-up method were estimated to decrease from 23000 in 2005 to 19973 Gg in 2012, with a peak value of 27061 Gg in 341 2008. In contrast, the number of fire points in YRD farmland increased from 7158 in 2005 to 17074 in 2012. The fire counts detected from satellite thus did not support the 342 effectiveness of OBB restriction by government in YRD before 2013. Table S10 in the 343 supplement presents the annual OBB emissions derived from FRP-based method for 344 2005-2015 in YRD region. Associated with fire counts, CO₂ emissions were estimated 345 to grow by 119.7% from 2005 to 2012, with the largest and the second largest annual 346 emissions calculated at 19977 and 12718 Gg for 2012 and 2010, respectively (Figure 347 3). Similar temporal variability was found for fire counts, which increased by 138.5% 348 349 from 2005 to 2012, with the most and the second most counts found at 17074 and 12322 for 2012 and 2010, respectively. 350

With the constraining method, as shown in Figure S5 in the supplement, the ratio 351 of constrained mass of CRBF for 2012 to 2010 was 1.51, clearly lower than the ratios 352 of original FRE (1.75) but close to the ratio of modified FRE for 2012 to 2010 (1.57). 353 The comparison suggested that modified FRE better reflect the OBB activity in YRD 354 than original FRE. In order to make the ratio of FRE for the two years be closer to the 355 ratio of constrained mass of CRBF, an improved method was developed for 356 calculating the FRE. Given the possible variation of FRP_{peak} hour between years, we 357 358 obtained the diurnal cycle of total FRP of YRD for 2005-2015 based on Gaussian fitting as shown in Figure S6 in the supplement. The ratio of FRE for 2012 to 2010 359 360 was recalculated at 1.54, further closer to the ratio of constrained mass of CRBF. Therefore the ratios of FRE for another given year to 2012 and 2010 were calculated 361 with this improved method, and were then applied to emission scaling for that year. 362 The constrained OBB emissions from 2005 to 2015 were summarized in Table 1. The 363 inter-annual trend in constrained emissions was similar with those in fire counts and 364 FRP-based emissions but different from that in emissions with traditional bottom-up 365 method, as shown in Figure 3. It is usually difficult to collect accurate percentages of 366 CRBF from bottom-up method, as it demands intensive investigation in the rural areas. 367 In addition, the percentages of CRBF were not updated for each year, and same 368 percentages were commonly applied for years without sufficient data support from 369 local surveys. 370

The constrained CO_2 emissions for Jiangsu, Anhui, Zhejiang and Shanghai were calculated at 5790, 4699, 1104 and 419 Gg in 2005, accounting for 48.2%, 39.1%, 9.2% and 3.5% of total OBB emissions in YRD, respectively. The analogue numbers for 2012 were 7345, 16159, 2574 and 394 Gg, and 27.7%, 61.0%, 9.7% and 1.5%,

respectively. Jiangsu and Anhui were found to contribute largest to OBB emissions in 375 YRD for 2005 and 2012, respectively. In the traditional bottom-up method, however, 376 Anhui was estimated to contribute largest for both years. City-level OBB emissions 377 estimated with the three methods were summarized in Table S11-S13 in the 378 supplement. With the constraining method, in particular, largest CO₂ emissions were 379 found in Suzhou (1708 Gg) of Anhui, Lianyungang (1578 Gg) and Xuzhou (1401 Gg) 380 of Jiangsu in 2005, accounting for 14.2%, 13.1% and 11.7% of the total emissions, 381 respectively. In 2012, Suzhou, Bozhou of Anhui, and Xuzhou of Jiangsu were 382 383 identified as the cities with the largest emissions, with the values estimated at 5007, 384 2433, and 2109 Gg, respectively. Depending on distribution of fire points, the shares of OBB emissions by city were close between constraining and FRP-based method, 385 and large emissions concentrated in the north of YRD. Based on surveyed percentages 386 of CRBF and crop production, in contrast, the emission shares by city in traditional 387 bottom-up method were clearly different from the other two, and emissions 388 concentrated in Anhui cities with high crop production level. 389

The average annual emissions of CO_2 for 2005-2011 with traditional bottom-up 390 method were 87.0% larger than those in constraining method and the emissions for 391 392 2012 was 24.6% times smaller than those in constraining method. Given the same sources of emission factors for all species except NMVOCs, the discrepancies of OBB 393 394 emissions for most species between constraining and traditional bottom-up methods come from the activity levels (i.e., percentages of CRBF and crop production). The 395 average annual constrained emissions from 2005 to 2015 were larger than those 396 derived by FRP-based method for all species except EC, CH₄ and NH₃, since the 397 average annual mass of CRBF from constraining method were 36.9% larger than 398 those from FRP-based method for these years, as shown in Figure S7. 399

The percentage of CRBF is an important parameter to judge OBB activity and to 400 estimate emissions. Besides the investigated values applied in traditional bottom-up 401 approach, the percentages of CRBF were recalculated based on the constrained 402 emissions at provincial level and were shown in Figure S8 in the supplement. The 403 largest and smallest percentages of CRBF in the whole YRD region were estimated at 404 18.3% in 2012 and 8.1% in 2006, respectively. The inter-annual trend in percentages 405 of CRBF for YRD was closest to that for Anhui province, as the province dominated 406 the crop burning in the region. The different inter-annual trends by province were 407 strongly influenced by agricultural practice and government management. 408

Agricultural practice could be associated with income level and mechanization level. 409 Increased income, would lead to more crop residues discarded and burned in the field, 410 while development of mechanization would lead to less. The constrained percentages 411 of CRBF for Shanghai increased from 2005 to 2007 and declined after 2007, while 412 those for Jiangsu decreased from 2005 to 2008 and increased after 2008. Increasing 413 trends were found for the percentages of CRBF for Anhui and Zhejiang from 2005 to 414 2012, and they might result largely from growth of farmers' income. Note that 415 percentages of CRBF for all provinces except Zhejiang decreased significantly in 416 417 2008, attributed largely to the measures of air quality improvement for Beijing Olympic Games. Shanghai was the only one with its percentage of CRBF 418 significantly reduced in 2010, resulting mainly from the air pollution control for 419 Shanghai World Expo in that year. Compare to the percentages of CRBF used in 420 bottom-up method, the constrained ones of Anhui and Jiangsu for all the years except 421 2012 were smaller, leading to lower constrained OBB emissions than bottom-up ones 422 in those years. 423

The constrained percentages of CRBF and straw yields for 2012 were shown by 424 city in Figure S9 in the supplement, and clear inconsistency in spatial distributions 425 426 can be found. The percentage of CRBF was not necessarily high for a city with large straw production. For instance, straw production of Yancheng was higher than most 427 428 other cities, but its percentage of CRBF was 5.7% and lower than most other cities. Through linear regression, correlation coefficient was calculated at only 0.06 between 429 constrained percentage of CRBF and straw yield at city level. The poor correlation 430 between them thus suggested that large uncertainty could be derived if uniform 431 percentage of CRBF was applied to calculate OBB emissions for cities within given 432 province, as what we did in the traditional bottom-up methodology. 433

434

3.2 Evaluation of the three OBB inventories with CMAQ

Figures 4 and 5 illustrate the observed 24-hour averaged and simulated hourly PM₁₀ concentrations for selected YRD cities in June 17-25, 2010 and June 8-14, 2012, respectively. Four emission cases, i.e., inventory without and with OBB emissions estimated using the three methods, were included. The simulated PM₁₀ concentrations without OBB emissions were significantly lower than observation for all cities, implying that OBB was an important source of airborne particulates during the two periods. Simulations with OBB emissions derived from the three methods performed

better than those without OBB emissions for most cities during June17-25, 2010 and 442 all cities during June 8-14, 2012. The best performance was found for simulations 443 with constrained OBB emissions in most cities during the two periods, and the high 444 PM₁₀ concentrations were generally caught by CTM for the concerned OBB events. In 445 2010, the observed high concentrations were simulated with constrained emissions in 446 447 Lianyungang during June 21-23, and Fuyang and Huainan during June 19-21. In 2012, the observed high concentrations were caught with constrained emissions in Xuzhou 448 during June 12-14, Lianyungang during June 13-14, Fuyang during June 11-12, 449 450 Bozhou during June 10 and Chuzhou during June 11-12. The results thus indicated that fire points could principally capture the temporal and spatial distribution of OBB 451 emissions. Overestimation still existed with constrained OBB emissions for the cities 452 with intensive fire points (e.g., Xuzhou, Bozhou and Fuyang in 2012 and Bengbu in 453 2010), while underestimation commonly existed for cities with fewer fire points (e.g., 454 Hefei, Chuzhou and Huainan in 2010 and 2012). Due to limitation of MODIS 455 observation, fires at moderate to small scales could not be fully detected (Giglio et al., 456 2003; Schroeder et al., 2008), thus the spatial allocation of OBB emissions based on 457 FRP could possibly result in more emissions than actual in areas with intensive fire 458 459 points. Moreover, we used both PM_{2.5} and PM₁₀ concentrations (which were available since 2013) to evaluate the model performances when the constrained, FRP-based or 460 461 no OBB emissions were applied in CTM for an OBB event during June 7-13, 2014. Figures S10 and S11 in the supplement illustrate the observed and simulated hourly 462 concentrations for PM_{2.5} and PM₁₀ in selected YRD cities, respectively. The best 463 performance was found for simulations with the constrained OBB emissions in most 464 cities during the periods, and the peak particle concentrations were generally caught 465 by CTM. The observed high concentrations were simulated with the constrained 466 emissions in Lianyungang and Sugian on June 12 and Huaian and Yancheng on June 467 13. 468

The NMB and NME between observed and simulated $PM_{2.5}$ and PM_{10} concentrations are shown in Table 2. In most cases, the NMB and NME with constrained OBB emissions were smaller than those with other OBB emissions, implying the best guess of OBB emissions obtained through the constraining method combining CTM and ground observation. The simulated $PM_{2.5}$ and PM_{10} concentrations using FRP-based OBB emissions were smaller than observation for the three periods, due mainly to the mass of CRBF were underestimated. The results thus 476 indicated that OBB emissions might be underestimated in FRP-based method in 2010, 2012 and 2014, since many small fires in YRD were undetected in MODIS active fire 477 detection products. The probability of MODIS detection was strongly dependent upon 478 the temperature and area of the fire being observed. The average probability of 479 detection for tropical savanna was 33.6% when the temperature of fire was between 480 600 and 800 °C and the area of fire was between 100 and 1000 m² (Giglio et al., 2003). 481 In YRD region, on one hand, the fire temperature of crop residue burned in fields was 482 relatively low. On the other hand, nearly 100 farmers were possibly located in a single 483 1×1 km MODIS pixel (Liu et al., 2015), and a famer commonly owned croplands of 484 several hundred square meters. Therefore many fire pixels in YRD might not be 485 486 detected, leading to underestimation in the total FRE. The simulated PM_{10} concentrations using traditional bottom-up OBB emissions were higher than 487 observation in 2010 but lower in 2012. The results thus implied the growth in OBB 488 emissions from 2010 to 2012 could not be captured by traditional bottom-up method, 489 490 attributed partly to application of unreliable percentage of CRBF. We further selected the performance of CMAQ modeling in US (Zhang et al., 2006) as the benchmark for 491 PM_{2.5} and PM₁₀ simulation. As can be seen in Table 2, the NMBs and NMEs for most 492 case with the constrained OBB emissions were close to those by Zhang et al. (2006). 493 The NMEs for hourly $PM_{2.5}$ and PM_{10} were slightly larger. Given the larger 494 495 uncertainty in emission inventory of anthropogenic sources for China and the uncertainty in spatial and temporal distribution of OBB emissions due to satellite 496 detection limit, we believe the model performance with the constrained OBB 497 emissions was improved and acceptable. 498

499 **3.3 Comparisons of different methods and studies**

We selected CO to compare emissions in this work and other inventories for 500 YRD, given the similar emission factors of CO applied in different studies. CO 501 502 emissions from the three methods in this study were compared with GFASv1.0 (Kaiser et al., 2012), GFEDv3.0 (van der Werf et al., 2010), GFEDv4.1 (Randerson et 503 504 al. 2018), Wang and Zhang (2008), Huang et al. (2012), Xia et al. (2016) and Zhou et al. (2017a), as shown in Figure 6. The emissions from Wang and Zhang (2008), 505 Huang et al. (2012), Xia et al. (2016) and Zhou et al. (2017a) were derived by 506 traditional bottom-up method, while GFASv1.0, GFEDv3.0 and GFEDv4.1 were 507 508 based on FRP and BA methods. In particular, emissions from small fires were included in GFEDv4.1. Similar inter-annual variations were found for emissions
derived from FRP measurement including the constrained and FRP-based emissions
in this work, GFAS v1.0, and GFED v4.1, while those of GFEDv3.0 and Xia et al.
(2016) were different. The percentages of CRBF were assumed unchanged during the
studying period in Xia et al. (2016), thus the temporal variation of OBB emissions
were associated with the change in annual straw production.

The constrained CO emissions in this work were lower than other studies using 515 traditional bottom-up method (Wang and Zhang, 2008; Huang et al., 2012; Xia et al., 516 517 2016) and higher than those based on burned area and FRP derived from satellite (GFEDv3.0; GFASv1.0; GFEDv4.1). In particular, the average annual constrained 518 emissions from 2005 to 2012 were 3.9, 0.5 and 15.0 times larger than those in 519 GFASv1.0, GFEDv4.1s and GFEDv3.0, respectively. The constrained emissions were 520 closest to GFED v4.1s that included small fires. Since the area of farmland belonging 521 to individual farmers was usually small, small fires were expected to be important 522 sources of OBB emissions in YRD. GFEDv4.1s might still underestimate OBB 523 emissions due to the omission errors for the small fires in MODIS active fire detection 524 products (Schroeder et al., 2008). In addition, the constrained CO emission for 2013 525 526 was 31.5% larger than those by Qiu et al. (2016) calculated based on burned area from satellite observations. The average annual CO emissions from 2005 to 2012 by the 527 constraining method were 57.2% smaller than Xia et al. (2016), and the constrained 528 emissions for 2006 were respectively 27.6% and 56.9% lower than those by Huang et 529 530 al. (2012) and Wang and Zhang (2008). It implied again that the emissions derived from traditional bottom-up method might be overestimated. Moreover, discrepancy in 531 estimations for the same year between Huang et al. (2012) and Wang and Zhang 532 (2008) with traditional bottom-up resulted mainly from application of different 533 percentages of CRBF, implying that calculation of OBB emissions was sensitive to 534 the parameter with the bottom-up approach. 535

The spatial distribution of constrained emissions in this work and those in GFASv1.0, GFEDv3.0 and GFEDv4.1s were illustrated in Figure 7. Intensive OBB emissions in GFEDv3.0 were mainly found in parts of Anhui, Jiangsu and Shanghai, while the constrained emissions, GFEDv4.1s and GFASv1.0 emissions occurred in most YRD regions in accordance with the distribution of fire points. Therefore, GFEDv3.0 might miss a large number of burned areas, leading to underestimation in emissions and bias in spatial distribution.

In order to understand the discrepancies of emissions for different species in this 543 work and other inventories, the emissions of 2010 derived from the three methods in 544 this study, GFASv1.0, GFEDv3.0, GFEDv4.1s and Xia et al. (2016) were summarized 545 in Table 3. Similar to CO, the constrained emissions for all species in this work were 546 lower than Xia et al. (2016) and OBB emissions of this study based on traditional 547 bottom-up method. The constrained emissions for all species in this work were larger 548 than GFASv1.0 and those for all species except NH₃ were larger than GFEDv3.0 and 549 GFEDv4.1s. In addition, the constrained emissions for most species were lower than 550 551 the emissions from Huang et al. (2012), Wang and Zhang (2008) and Xia et al. (2016) using traditional bottom-up method in 2006. In most cases, the discrepancy in activity 552 levels between studies was larger than that in emission factors. Specifically, the OBB 553 emissions for all species in FRP-based (WSE) were smaller than those derived by 554 bottom-up method. The differences in OBB emissions between bottom-up and 555 FRP-based (WSE) method were larger than 50% of those between the bottom-up and 556 the original FRP-based method with different emission factors for most species. It 557 indicated that the discrepancy in activity levels contributed the most to the difference 558 in OBB emissions between the two methods. 559

560 Resulting from the different sources of emission factors, the discrepancies between studies or methods varied greatly by species. For PM₁₀ and PM_{2.5}, as an 561 example, the emissions by Xia et al. (2016) were respectively 35.8% and 50.3% 562 higher than constrained emissions in 2010. The discrepancies for SO₂ and NO_X were 563 larger: the emissions by Xia et al. (2016) were 4.7 and 3.1 times larger than our 564 constrained emissions, respectively. Moreover, the constrained NMVOCs emission 565 was 152.5 and 10.7 times larger than that of GFEDv3.0 and GFEDv4.1s in 2010, as 566 the emission factors of GFEDv3.0 and GFEDv4.1s did not contain oxygenated VOCs. 567 In contrast, the constrained NH₃ emission was 4.7% and 47.9% smaller than that of 568 GFEDv3.0 and GFEDv4.1s. The comparisons indicated that emission factors were 569 important sources of uncertainties in estimation of OBB emissions with different 570 methods. 571

572 **3.4** Contribution of OBB to particulate pollution and its influencing factors

The brute-force method (BFM, Dunker et al., 1996) was used to analyze the contributions of OBB to PM_{10} pollution for the two OBB events, June 17-24, 2010 and June 8-14, 2012. Simulated PM_{10} concentrations with and without constrained 576 OBB emissions were compared, and the difference indicated the contribution from OBB as shown by city in Figure 8. The average contribution in June 8-14, 2012 was 577 estimated at 37.6% (56.7 μ g/m³) for 22 cities in YRD, and the contribution for June 578 17-24, 2010 was smaller at 21.8 % (24.0 μ g/m³) for 17 cities. Our result for 2012 was 579 nearly the same as that for 5 YRD cities in 2011 (37.0%) by Cheng et al. (2014). 580 Using the BFM method, the contribution of OBB emissions to PM₁₀ concentrations 581 were estimated to increase by 136.3% from 2010 to 2012 in this work, and the growth 582 rate was larger than that of OBB emissions (50.8%). Therefore, factors other than 583 emissions (e.g., meteorology) could also play an important role in elevating the 584 contribution of OBB to ambient particle pollution. For example, the average 585 precipitation in June 8-14, 2012 was 36% lower than that in June 17-24, 2010, 586 exaggerating the particle pollution during OBB event. For the OBB event during June 587 7-13, 2014, the contributions of OBB to both PM_{2.5} and PM₁₀ concentrations were 588 shown by city in Figure 9. The average contributions of $PM_{2.5}$ and PM_{10} were 589 estimated at 29% and 23% for 22 cities in YRD, indicating again that the OBB was an 590 important source of ambient particles. OBB contribution to PM₁₀ for 2014 was 591 smaller than that for 2012, attributed mainly to the reduced straw burning in crop 592 593 land.

The average contributions of OBB for 2012 were estimated at 55.0% (98.4 594 μ g/m³), 36.4% (58.0 μ g/m³), 23.6% (12.9 μ g/m³), and 14.4% (11.2 μ g/m³) for 6 595 cities of Anhui, 10 cities of Jiangsu, 5 cities of Zhejiang and Shanghai, respectively. 596 597 For individual cities, large contributions of OBB for 2012 were found in Xuzhou, Bozhou, Fuyang, and Lianyungang located in north YRD, reaching 82.3% (284.3 598 $\mu g/m^3$), 75.2% (207.5 $\mu g/m^3$), 71.9% (134.7 $\mu g/m^3$) and 63.5% (96.2 $\mu g/m^3$), 599 respectively. Similarly, large contributions for 2010 were found in Lianyungang, 600 Fuyang and Bozhou reaching 63.3% (69.8 μ g/m³), 58.2% (71.9 μ g/m³) and 78.8% 601 (53.6 μ g/m³), respectively. In general the spatial distribution of contributions to PM₁₀ 602 mass concentrations was similar with that of fire points, confirming the rationality of 603 constraining OBB emissions with observed PM₁₀ concentration in cities in north 604 Anhui and Jiangsu. For PM_{2.5}, the large contributions of OBB were found in Xuzhou, 605 Huaian and Suqian during the event in 2014, reaching 67.5% (111.7 μ g/m³), 60.7% 606 $(50.6 \,\mu\text{g/m}^3)$ and 53.2% (49.6 $\mu\text{g/m}^3$), respectively. 607

To explore the influence of meteorology on air pollution caused by OBB, we simulated PM_{10} concentrations for June 8-14 (PE1) and June 22-28 2012 (PE2) with

610 varied meteorology conditions but fixed OBB emissions (i.e., constrained emissions for June 8-14, 2012). Poorer meteorology conditions during PE1 were found than PE2. 611 The average wind speed in PE1 was 2.4 m/s, 17% lower than that in PE2. The average 612 wind direction in PE1 was 168.3°, close to south with polluted air in land. In contrast, 613 the average wind direction in PE2 was 118.3°, close to east with clean air from the 614 ocean. The average precipitation in PE2 was 6.8mm, 28% higher than that in PE1. As 615 shown in Figure 10, the average contribution of OBB to PM₁₀ concentrations for 22 616 cities in YRD region was estimated at 56.7 μ g/m³ for PE1, 23% larger than that for 617 PE2, and the contributions in most cities were much larger for PE1 than those for PE2, 618 except for Bozhou and Fuyang. The comparisons thus suggest that air pollution 619 caused by OBB would exaggerate under poorer meteorology conditions. To reduce air 620 pollution caused by OBB in harvest season in YRD, therefore, more attention should 621 be paid to the OBB restriction on those days with unfavorable meteorology conditions 622 such as calm wind and rainless period. 623

To further analyze the influence of diurnal variation of emissions on air pollution 624 caused by OBB, we simulated PM₁₀ concentrations of June 17-24 2010 with various 625 diurnal curves of OBB emissions (i.e., those for 2010 and 2012). Constrained 626 627 emissions were applied in the simulation. As shown in Figure 11, the contributions of OBB to PM₁₀ concentrations based on diurnal curve of 2012 were larger than those 628 based on 2010 for almost all YRD cities, and the average contribution for the 17 cities 629 was calculated at 28.6 μ g/m³ based on diurnal curve of 2012, 10% larger than that 630 based on 2010. The contribution in Bozhou changed most (1.37 times larger with 631 2012 curve), while those in Shanghai, Huzhou and Shaoxing changed least. The time 632 of peak value for OBB emissions in 2012 was 2.5 hours later than 2010, indicating 633 that the fraction of OBB emissions at night for 2012 would be larger than that for 634 2010. As the diffusion condition for air pollutants at night was usually worse than that 635 during daytime, more OBB emissions at night would elevate its contribution to 636 particle pollution. In the actual fact, the supervision of OBB prohibition was usually 637 conducted by government during daytime, thus some farmers burned more crop 638 residues at night to avoid the punishment. To improve the air quality in harvest season 639 in YRD, more attention should be paid to the OBB restriction at night. 640

641 **3.5 Uncertainty analysis**

The uncertainties of OBB emissions estimated with bottom-up and FRP-based methods were quantified by species using a Monte-Carlo simulation for 2012. A total of 20,000 simulations were performed and the uncertainties were expressed as 95% confidence intervals (CIs) around the central estimates. The parameters contributing most to OBB emission uncertainty were also identified according to their contribution to the variance in Monte-Carlo simulation.

For traditional bottom-up method, parameters included crop productions, 648 percentages of CRBF, straw to grain ratios, combustion efficiencies, and emission 649 650 factors. Crop production was directly taken from official statistical yearbooks (NBS, 2013) and its uncertainty was expected to be limited and not included in the analysis. 651 As the percentage of CRBF was determined at half of the percentage of unused crop 652 residues, its uncertainty was set at -100% to +100%. The combustion efficiencies 653 were assumed within an uncertainty range of 10% around the mean value according to 654 de Zarate (2005) and Zhang et al. (2008). Uncertainties of emission factors were 655 obtained from original literatures where they were derived. If emission factor was 656 derived from a single measurement, normal distribution was applied with standard 657 deviation directly taken from that work. If emission factor was derived from multiple 658 659 measurements and the samples were insufficient for data fitting, uniform distribution was tentatively applied with a conservative strategy to avoid possible underestimation 660 661 of uncertainty: The uncertain range of given emission factor would be expanded according to Li et al. (2007) if the range originally from multiple studies was smaller 662 than that in Li et al. (2007). Summarized in Table S14 in the supplement was a 663 database for emission factors and percentages of CRBF, with their uncertainties 664 indicated by probability distribution function (PDF). As shown in Table 4, the 665 uncertainties of OBB emissions with traditional bottom-up method for PM₁₀, PM_{2.5}, 666 EC, OC, CH₄, NMVOCs, CO, CO₂, NO_X, SO₂ and NH₃ in 2012 were estimated at 667 -56% to +70%, -56% to +70%, -50% to +54%, -54% to +73%, -49% to +58%, -48% 668 to +59%, -46% to +73%, -48% to +60%, -47% to +87%, -59% to +138% and -51% to 669 +67%, respectively. For most species, the percentages of CRBF contributed largest to 670 the uncertainties of OBB emissions, while emission factors were more significant to 671 SO₂ uncertainty. 672

For FRP-based method, parameters included total FRE, combustion conversion
ratio and emission factors. Uncertainty of total FRE was associated with FRP value,
MODIS detection resolution, and the methodology used to calculate FRE per fire

pixel. Indicated by Freeborn et al. (2014), the coefficient of variation of MODIS FRP 676 for a fire pixel was 50%, but it declined to smaller than 5% for the aggregation of over 677 50 MODIS active fire pixels. Give the large number of fire pixels for in YRD (more 678 than 17000 in 2012), FRP was expected to contribute little to uncertainty of total FRE 679 and could thus be ignored. Due to limitation of MODIS resolution, small fires could 680 not be fully detected and the number of fire pixel could be underestimated by 300% 681 on crop-dominant areas (Schroeder et al., 2008), therefore the uncertainty of number 682 of fire pixel was assumed to be 0 to +300%. The method used to calculate FRE based 683 684 on single fire pixel assumed that fire lasted one day. Given the small cropland owned by one farmer in YRD, individual fire normally lasted several hours, and FRE could 685 be overestimated. As the total FRE in FRP-based method was estimated 2.6 times 686 larger than that from constraining method based on the same number of the fire pixel, 687 we tentatively assumed the uncertainty range of FRE for one fire pixel at 0% to -72%. 688 The uncertainty of total FRE was then estimated at -17% to +154% (95% CIs) based 689 on the principle that total FRE was calculated as the number of fire pixel multiplied 690 by average FRE. The uncertainty of combustion conversion ratio was derived from 691 Wooster et al. (2005) and Freeborn et al. (2008), while those of emission factors taken 692 693 from Akagi et al. (2011). As a result, uncertainties of FRP-based inventory were estimated at -77% to +274%, -63% to +244%, -78% to +281%, -78% to 276%, -83% 694 695 to +315%, -63% to +243%, -52% to +223%, -21% to +164%, -82% to +303%, -78% to +279%, and -82% to +302% for PM₁₀, PM_{2.5}, EC, OC, CH₄, NMVOCs, CO, CO₂, 696 NO_X, SO₂ and NH₃ in 2012, respectively. Emission factors contributed most to the 697 uncertainties of emissions for all species except CO₂. 698

The uncertainty of constrained emissions could hardly be provided by 699 Monte-Carlo simulation, as the results were associated with CTM performance. In 700 general, CTM performance could be influenced by emission estimates for sources 701 other than OBB, chemistry mechanism of CTM and temporal and spatial distribution 702 of OBB emissions. Emission inventory of anthropogenic sources that incorporates the 703 best available information of individual plants was expected to improve the CTM 704 performance at the regional or local scale (Zhou et al., 2017b). The influence of 705 chemistry mechanism came mainly from secondary organic carbon (SOC) modeling. 706 According to the Cheng et al. (2014) and Chen et al. (2017), the mass fraction of SOC 707 to PM₁₀ could reach 10% during the OBB event in YRD, and that part might not be 708 well constrained with the approach we applied in this work. Similar to FRP-based 709

method, moreover, temporal and spatial distribution of OBB emissions based on FRP might not be entirely consistent with the reality, due to omission errors in the MODIS active fire detection products and limited times of satellite overpass as discussed earlier. Due to data limitation, finally, we relied on available PM_{10} concentrations in current method. More data of multi pollutant concentrations (e.g., $PM_{2.5}$, OC and EC) with sufficient temporal and spatial resolution are in great need to better constrain the OBB emissions.

In general, uncertainties of OBB emissions with traditional bottom-up method 717 718 were estimated smaller than those with FRP-based method, and uncertainties for CO_2 and CO were usually smaller than other species in both methods attributed mainly to 719 fewer variations in their emission factors. OBB emission estimation with traditional 720 bottom-up method could be improved if more accurate percentages of CRBF are 721 obtained, and that with FRP-based method could be improved when the omission 722 error of satellite and the uncertainties of emission factors are reduced. Efforts should 723 also be recommended on improvement of CTM for better constraining the OBB 724 emissions. 725

726

727

4. Conclusions

728 Taking YRD in China as an example, we have thoroughly analyzed the discrepancies and their sources of OBB emissions estimated with traditional 729 bottom-up, FRP-based and constraining methods. The simulated PM₁₀ concentrations 730 through CMAQ with constrained emissions were closest to available observation, 731 implying the improvement of emission estimation with this method. The inter-annual 732 733 variations in emissions with FRP-based and constraining methods were similar with the fire counts, while that with traditional bottom-up method was not. It indicated that 734 emissions with traditional bottom-up method could not capture the real inter-annual 735 trend of OBB emissions. The emissions of all species except NMVOCs based on 736 737 traditional bottom-up method might be overestimated in most years, attributed mainly 738 to the elevated percentages of CRBF used in the method. The emissions with FRP-based method might be underestimated in 2005-2015, attributed to the omission 739 740 errors in the MODIS active fire detection products and thereby to the underestimation in mass of CRBF. The CO emissions with traditional bottom-up, FRP-based and 741 742 constraining methods were compared with other studies. Similar temporal variations

were found for the constrained emissions, emissions based on FRP-based, and 743 emissions in GFASv1.0 and GFEDv4.1s. CO emissions based on traditional 744 bottom-up method both in this work and other studies were usually higher than those 745 derived by constraining method, and the CO emissions based on FRP-based method 746 both in this work and other studies usually were lower than those derived by 747 748 constraining method. It again demonstrated that traditional bottom-up method might overestimate OBB emissions in YRD and FRP-based method might underestimate 749 them. The contributions of OBB to particulate pollution in typical episodes were 750 751 analyzed using the Brute-force method in CMAQ modeling. The OBB emissions in 2012 were 51% larger than those in 2010, while its contribution to average PM_{10} mass 752 concentrations was estimated to increase by 136% from 2010 to 2012. It indicated that 753 the elevated contribution of OBB was not attributed only to growth in OBB emissions 754 but was also influenced by the meteorology. Quantified with a Monte-Carlo 755 framework, the uncertainties of OBB emissions with traditional bottom-up method 756 were smaller than those with FRP-based method. The uncertainties of emissions based 757 on traditional bottom-up and FRP-based were mainly from the percentages of CRBF 758 and emission factors, respectively. Further improvement on CTM for OBB events 759 760 would help better constraining OBB emissions.

Limitations remained in this study. Given the difficulty in field investigation, 761 762 annual CRBF used in traditional bottom-up method was obtained from limited studies and it could not correctly reflect the real OBB activity. The reliability of OBB 763 emissions with FRP-based method depended largely on the detection resolution of the 764 satellite. In YRD where the burned areas of individual fires were small, many fires 765 could not be detected by MODIS. The accuracy of constrained emissions depended 766 largely on model performance and spatial and temporal distributions of OBB 767 emissions derived from satellite-observed FRP. Therefore FRP-based and constraining 768 method may be improved if more reliable fire information is obtained. In addition, 769 more measurements on local emission factors for OBB are suggested in the future to 770 reduce the uncertainty of emissions. 771

772

773

Acknowledgements

This work was sponsored the National Key Research and Development Program of China (2016YFC0201507 and 2017YFC0210106), Natural Science Foundation of

China (91644220 and 41575142), Natural Science Foundation of Jiangsu
(BK20140020), and Special Research Program of Environmental Protection for
Common wealth (201509004). The MCD14ML data were provided by LANCE
FIRMS operated by the NASA/GSFC/Earth Science Data and Information System
(ESDIS) with funding provided by NASA/HQ.

781

782

References

- Akagi, S., Yokelson, R. J., Wiedinmyer, C., Alvarado, M., Reid, J., Karl, T., Crounse,
 J., and Wennberg, P.: Emission factors for open and domestic biomass burning for use
 in atmospheric models, Atmos. Chem. Phys. 11 (9), 4039-4072, 2011.
- Andreae, M. O., and Merlet, P.: Emission of trace gases and aerosols from bio
 mass burning, Glob. Biogeochem. Cy. 15(4), 955-966. <u>http://dx.doi.org/10.1029/2</u>
 000gb001382, 2001.
- Bi, Y. Y.: Study on straw resources evaluation and utilization, Chinese AcademyAgriculture Sciences, Beijing, China, 2010 (in Chinese).
- Cao, G. L., Zhang, X. Y., Wang, D., and Zheng, F. C.: Inventory of atmospheric
 pollutants discharged from open biomass burning in China continent, Chinese Science
 Bulletin, 52(15):1826-1831, 2007 (in Chinese).
- Chen, D., Cui H. F., Zhao Y., Yin L., Lu, Y., Wang, Q. G.: A two-year study of
 carbonaceous aerosols in ambient PM 2.5 at a regional background site for western
 Yangtze River Delta, China, Atmos. Res., 183, 351-361, 2017.

Cheng, Z., Wang, S.X., Fu, X., Watson, J.G., Jiang, J., Fu, Q., Chen, C., Xu, B., Yu, J.,
Chow, J.C., and Hao, J.: Impact of biomass burning on haze pollution in the Yangtze
River delta, China: a case study in summer 2011, Atmos. Chem. Phys., 14, 4573-4585,
2014.

- Cheng, Z., Wang, S.X., Jiang, J. K., Fu, Q.Y., Chen, C.H., Xu, B.Y., Yu J.Q., Fu, X.,
 and Hao J.M.: Long-term trend of haze pollution and impact of particulate matter in
 the Yangtze River Delta, China, Environ. Pollut., 182, 101-110, 2013.
- Crutzen, P. J., and Andreae, M. O.: Biomass burning in the tropics: Impact on
 atmospheric chemistry and biogeochemical cycles, Science, 250 (4988), 1669-1678,
 1990.
- Bor Davies, D. K., Ilavajhala, S., Wong, M. M., and Justice, C. O.: Fire Information for
 Resource Management System: Archiving and Distributing MODIS Active Fire Data,
 IEEE Geosci. Remote Sens., 47, 72-79, 2009.
- de Zarate, I. O., Ezcurra, A., Lacaux, J. P., Van Dinh, P., de Argandona, J. D.:
 Pollution by cereal waste burning in Spain, Atmos. Environ., 73, 161~170, 2005.
- B12 Dunker, A. M., Morris, R. E., Pollack, A. K., Schleyer, C. H., and Yarwood, G.:
 Photochemical modeling of the impact of fuels and vehicles on urban ozone using
 auto oil program data, Environ. Sci. & Technol., 30, 787–801, 1996.
- Emery, C., Tai, E., and Yarwood, G.: Enhanced meteorological modeling and performance evaluation for two Texas episodes, Report to the Texas Natural

- Resources Conservation Commission, prepared by ENVIRON, International Corp.Novato, CA, 2001.
- 819 European Space Agency and Université Catholique de Louvain, GLOBCOVER
- 2009 Products Description and Validation Report, 2011, Available online: http://
 due.esrin.esa.int/files/GLOBCOVER2009_Validation_Report_2.2.pdf.

Fu, X., Wang, S.X., Zhao, B., Xing, J., Cheng, Z., Liu, H., and Hao, J. M.: Emission
inventory of primary pollutants and chemical speciation in 2010 for the Yangtze River
Delta region, China, Atmos. Environ., 70, 39-50, 2013.

- Freeborn, P. H., Wooster, M. J., Roy, D. P., Cochrane, M. A.: Quantification of
 MODIS fire radiative power (FRP) measurement uncertainty for use in satellite based
 active fire characterization and biomass burning estimation, Geophys. Res. Lett.,
 41(6), 1988-1994, 2014.
- Freeborn, P. H., Wooster, M. J., Hao, W. M., Ryan, C. A., Nordgren, B. L., Baker, S. P.,
 and Ichoku, C.: Relationships between energy release, fuel mass loss, and trace gas
 and aerosol emissions during laboratory biomass fires, J. Geophys. Res., 113, D01301.
 http://dx.doi.org/10.1029/2007jd008679, 2008.
- Giglio, L., Randerson, J. T., and van der Werf, G. R.: Analysis of daily, monthly, and
 annual burned area using the fourth generation global fire emissions database
 (GFED4), J. Geophys. Res.: Biogeo., 118, 317–328, doi:10.1002/jgrg.20042, 2013.
- Giglio, L., Descloitres, J., Justice, C. O., Kaufman Y. J.: An enhanced contextual fire
 detection algorithm for MODIS, Remote Sens. Environ., 87(2-3): 273-282, 2003.
- Guo, H., Cheng, T., Gu, X., Wang, Y., Chen, H., Bao, F., Shi, S. Y., Xu, B. R., Wang,
 W. N., Zuo, X., Zhang, X. C., Meng, C.: Assessment of pm_{2.5} concentrations and
 exposure throughout china using ground observations, Sci. Total Environ., 1024,
 601-602, 2017.
- Hodzic A., Duvel J. P.: Impact of biomass burning aerosols on the diurnal cycle of
 convective clouds and precipitation over a tropical island, J. Geophys. Res., 123,
 1017–1036. https://doi.org/10.1002/2017JD027521, 2018.
- Hooghiemstra, P. B., Krol, M. C., vanLeeuwen, T. T., van der Werf, G. R., Novelli, P.
 C., Deeter, M. N., Aben, I., and Röckmann, T.: Interannual variability of carbon
 monoxide emission estimates over South America from 2006 to 2010, J. Geophys.
 Res., 117, D15308, doi:10.1029/2012JD017758, 2012.
- Huang, X., Ding, A. J., Liu, L. X., Liu, Q., Ding, K., Nie, W., Xu, Z., Chi, X. G.,
 Wang, M. H., Sun, J. N., Guo, W. D., and Fu, C. B.: Effects of aerosol-radiation
 interaction on precipitation during biomass-burning season in East China, Atmos.
 Chem. Phys. Discuss., doi: 10.5194/acp-2016-272, 2016.
- Huang, X., Li M., Li, J., Song, Y.: A high-resolution emission inventory of crop
 burning in fields in China based on MODIS Thermal Anomalies/Fire products, Atmos.
 Environ., 50(3), 9-15, 2012.
- Jiangsu Provincial Development and Reform Commission (JPDRC), and Jiangsu
 Provincial Agricultural Commission (JPAC): Comprehensive utilization planning of
 crop straw in Jiangsu, Nanjing, China, 2009 (in Chinese).
- Jiménez, P., Jorba, O., Parra R. and Baldasano J. M.: Evaluation of MM5-EMICAT2000-CMAQ performance and sensitivity in complex terrain:

High-resolution application to the northeastern Iberian Peninsula, Atmos. Environ., 40,
5056-5072, doi:10.1016/j.atmosenv.2005.12.060, 2006.

Kaiser, J. W., Heil, A., Andreae, M. O., Benedetti, A., Chubarova, N., Jones, L., 863 Morcrette, J. J., Razinger, M., Schultz, M. G., Suttie, M., and van der Werf, G. R.: 864 Biomass burning emissions estimated with a global fire assimilation system based on 865 observed fire radiative power. Biogeosciences, 9. 527-554. doi: 866 10.5194/bg-9-527-2012, 2012. 867

Konovalov, B., Berezin, E. V., Ciais, P., Broquet, G., Beekmann, M., Hadji-Lazaro, J.,
Clerbaux, C., Andreae, M. O., Kaiser, J. W., and Schulze, E.-D.: Constraining CO₂
emissions from open biomass burning by satellite observations of co-emitted species:
a method and its application to wildfires in Siberia, Atmos. Chem. Phys., 14,
10383–10410, 2014.

Krol, M., Peters, W., Hooghiemstra, P., George, M., Clerbaux, C., Hurtmans, D.,
McInerney, D., Sedano, F., Bergamaschi, P., El Hajj, M., Kaiser, J. W., Fisher, D.,
Yershov, V., and Muller, J.-P.: How much CO was emitted by the 2010 fires around
Moscow?, Atmos. Chem. Phys., 13, 4737–4747, doi: 10.5194/acp-13-4737-2013,
2013.

- Li, J. F., Song, Y., Mao, Y., Mao, Z. C., Wu, Y. S., Li, M. M., Huang, X., He, Q. C.,
 and Hu, M.: Chemical characteristics and source apportionment of PM_{2.5} during the
 harvest season in eastern China's agricultural regions, Atmos. Environ., 92, 442–448,
 doi: 10.1016/j.atmosenv.2014.04.058, 2014.
- Li, X. H., Wang, S. X., Duan, L., Hao, J. M., LiC., Chen, Y. S., and Yang, L.: Particulate and trace gas emissions from open burning of wheat straw and corn stover in China, Environ. Sci.& Technol., 41, 6052-6058, 2007.
- Liu, M. X., Song, Y., Yao H., Kang, Y. N., Li, M. M., Huang, X., and Hu, M.: Estimating emissions from agricultural fires in the North China Plain based on MODIS fire radiative power, Atmos. Environ., 112, 326–334, 2015.
- National Bureau of Statistics (NBS): China Statistical Yearbook 2006-2013, China
 Statistics Press, Beijing, 2013 (in Chinese).
- National Development and Reform Commission Office (NDRC), and National
 Environmental Protection Department (NEPD): Comprehensive utilization and
 burning of crop straw in China, Beijing, China, 2014 (in Chinese).
- Price, C., Penner, J., and Prather, M.: NO_x from lightning, Part I: Global distri
 bution based on lightning physics, J. Geophys. Res.-Atmos., 102, D5, doi: 10.1
 029/96JD03504, 1997.
- Qiu, X. H., Duan, L, Chai F. H. Wang S. X., Yu Q., and Wang S. L.: Deriving
 high-resolution emission inventory of open biomass burning in China based on
 satellite observations, Environ. Sci. Technol., 50 (21), 11779–11786. DOI:
 10.1021/acs.est.6b02705, 2016.

Ran, L., Zhao, C., Geng, F., Tie, X., Peng, L., Zhou, G., Yu, Q., Xu, J., and
Guenther, A.: Ozone photochemical production in urban Shanghai, China: Anal
ysis based on groud level observations, J. Geophys. Res., 114, D15301, doi: 10.
1029/2008JD010752, 2009.

- Randerson, J. T., van der Werf, G. R., Giglio, L., Collatz, G. J., and Kasibhatla, P. S.:
 Global Fire Emissions Database, Version 4.1, (GFEDv4), ORNL DAAC, Oak Ridge,
 Tennessee, USA. http://dx.doi.org/10.3334/ORNLDAAC/1293, 2018.
- Richter, A., Burrows, J. P., Nuss, H., Granier, C., and Niemeier, U.: Increase in tropospheric nitrogen dioxide over China observed from space, Nature, 437, 129-132, 2005.
- Schroeder, W., Prins, E., Giglio, L., Csiszar, I., Schmidt, C., Morisette, J., and
 Morton, D.: Validation of GOES and MODIS active fire detection products usi
 ng ASTER and ETM+ data, Remote Sens. Environ, 112 (5), 2711-2726, http://
 dx.doi.org/10.1016/j.rse.2008.01.005, 2008.
- Shi, Y. S., and Yamaguchi, Y.: A high-resolution and multi-year emissions inventory
 for biomass burning in Southeast Asia during 2001-2010, Atmos. Environ., 98 (98):
 8-16, 2014.
- Sindelarova, K., Granier, C., Bouarar, I., Guenther, A., Tilmes, S., Stavrakou, T.,
 Müller, J.-F., Kuhn, U., Stefani, P., and Knorr, W.: Global data set of biogenic VOC
 emissions calculated by the MEGAN model over the last 30 years, Atmos. Chem.
 Phys., 14, 9317–9341, doi: 10.5194/acp-14-9317-2014, 2014.
- Streets, D. G., and Yarber, K. F.: Biomass burning in Asia: Annual and seasonal
 estimates and atmospheric emissions, Global Biogeochemical Cycles, 17, 4, 1099, doi:
 10.1029/2003GB002040, 2003.
- Su, J. F., Zhu B., Kang, H. Q., Wang, H. N., and Wang T. J.: Applications of pollutants
 released form crop residues at open burning in Yangtze River Delta, Environmental
 Science, 5, 1418-1424, 2012 (in Chinese).
- van der Werf, G. R., Randerson, J. T., Giglio, L., Collatz, G. J., Mu, M., Kasi
 bhatla, P. S., Morton, D. C., DeFries, R. S., Jin, Y., and van Leeuwen, T. T.:
 Global fire emissions and the contribution of deforestation, savanna, forest, agri
 cultural, and peat fires (1997-2009), Atmos. Chem. Phys., 10, 11707-11735, doi:
 10.5194/acp-10-11707-2010, 2010.
- Van Donkelaar, A., Martin, R. V., Brauer, M., Kahn, R., Levy, R., Verduzco, C., and
 Villeneuve, P. J.: Global estimates of ambient fine particulate matter concentrations
 from satellite-based aerosol optical depth: development and application, Environ.
 Health. Persp., 118, 847-855, 2010.
- Vermote, E., Ellicott, E., Dubovik, O., Lapyonok, T., Chin, M., Giglio, L., and
 Roberts, G.J.: An method to estimate global biomass burning emissions of organic and
 black carbon from MODIS fire radiative power, J. Geophys. Res. 114 (D18)
 http://dx.doi.org/10.1029/2008jd011188, 2009.
- Wang, S. X., and Zhang, C. Y.: Spatial and temporal distributions of air pollutant
 emissions from open burning of crop residues in China, Sciencepaper Online,
 5(5):329-333, 2008 (in Chinese).
- Wiedinmyer, C., Akagi, S. K., Yokelson, R. J., Emmons, L. K., Al- Saadi, J. A.,
 Orlando, J. J., and Soja, A. J.: The Fire Inventory from NCAR (FINN): a high
 resolution global model to estimate the emissions from open burning, Geosci. Model
 Dev., 4, 625–641, doi: 10.5194/gmd-4-625-2011, 2011.
- Wooster, M. J., Roberts, G., Perry, G. L. W., and Kaufman, Y. J.: Retrieval of biomass
 combustion rates and totals from fire radiative power observations: FRP derivation

- and calibration relationships between biomass consumption and fire radiative energy
 release, J. Geophys. Res., 110, D24. http://dx.doi.org/10.1029/2005jd006318, 2005.
- Xia, Y. M., Zhao Y., Nielsen, C. P.: Benefits of China's efforts in gaseous pollutant
 control indicated by the traditional bottom-up emissions and satellite observations
 2000-2014, Atmos. Environ., 136: 43-53, 2016.
- Xiao, Z. M., Zhang, Y. F., Hong, S. M., Bi, X. H., Jiao, L., Feng, Y. C., and Wang, Y.
 Q.: Estimation of the main factors influencing haze, based on a long-term monitoring
 Campaign in Hangzhou, China. Aerosol Air Qual. Res., 11, 873-882, 2011.
- Xing, J., Mathur, R., Pleim, J., Hogrefe, C., Gan, C. -M., Wong, D. C., Wei, C.,
 Gilliam, R. and Pouliot, G.: Observations and modeling of air quality trends over
 1990–2010 across the Northern Hemisphere: China, the United States and Europe,
 Atmos. Chem. Phys., 15, 2723-2747, 2015.
- Zhang, H. F., Ye, X. G., Cheng, T. T., Chen, J. M., Yang, X., Wang, L., and Zhang, R.
 Y.: A laboratory study of agricultural crop residue combustion in China: Emission factors and emission inventory, Atmos. Environ., 42, 8432-8441, 2008.
- Zhang, Y., Liu, P., Pun, B., and Seigneur, C.: A comprehensive performance
 evaluation of MM5-CMAQ for the Summer 1999 Southern Oxidants Study
 episode-Part I: Evaluation protocols, databases, and meteorological predictions,
 Atmos. Environ., 40, 4825–4838, 2006.
- Zhao Y., Zhang J., and Nielsen C.P.: The effects of recent control policies on trends in
 emissions of anthropogenic atmospheric pollutants and CO₂ in China, Atmos. Chem.
 Phys., 13, 487-508, 2013.
- Zheng, Y., Xue, T., Zhang, Q., Geng, G., Tong, D., Li, X. and He, K. B.: Air quality
 improvements and health benefits from China's clean air action since 2013, Environ.
 Res. Lett., 12, 114020, 2017.
- Zhou Y., Xing X. F., Lang J. L., Chen D. S., Cheng S. Y., Wei L., Wei X., and Liu C.:
 A comprehensive biomass burning emission inventory with high spatial and temporal
 resolution in China, Atmos. Chem. Phys., 17, 2839–2864, 2017a.
- 277 Zhou, Y. D., Zhao Y., Mao P., Zhang Q, Zhang J., Qiu, L. P., and Yang, Y.:
 278 Development of a high-resolution emission inventory and its evaluation and
 279 application through air quality modeling for Jiangsu Province, China, Atmos. Chem.
 280 Phys., 17, 211–233, 2017b.

FIGURE CAPTIONS

Figure 1. (a) spatial patterns of fire points in June 2010 and June 2012, (b) PM_{10} 982 concentrations for city-level in YRD in June 2010 and June 2012, and (c) 983 temporal variations of daily fire occurrences in June 2010 and 2012. City 984 abbreviations FY, BZ, BB, HN, HF, CZ(a), XZ, LYG, NJ, YZ, ZJ, TZ, NT, CZ, 985 WX, SZ, HZ(a), JX, HZ, SX, NB, SH indicate is Fuyang, Bozhou, Bengbu, 986 Huainan, Hefei, Chuzhou, Xuzhou, Lianyungang, Nanjing, Yangzhou, Zhenjiang, 987 Taizhou, Nantong, Changzhou, Wuxi, Suzhou, Huzhou, Jiaxing, Hangzhou, 988 989 Shaoxing, Ningbo, and Shanghai.

Figure 2. Model domain and locations of 43 meteorological monitoring sites. The
numbers of 1-41 represent the cities of Fuyang, Bozhou, Huaibei, Suzhou,
Huainan, Bengbu, Luan, Hefei, Chuzhou, Anqing, Chaohu, Maanshan, Chizhou,
Tongling, Wuhu, Huangshan, Xuancheng, Xuzhou, Lianyungang, Suqian,
Huaian, Yancheng, Yangzhou, Taizhou, Nanjing, Zhenjiang, Nantong,
Changzhou, Wuxi, Suzhou; Huzhou, Jiaxing, Hangzhou, Shaoxing, Ningbo,
Zhoushan, Quzhou, Jinhua, Taizhou, Lishui and Wenzhou, respectively.

Figure 3. Fire counts and CO₂ emissions estimated with traditional bottom-up,
FRP-based and constraining methods for YRD 2005-2012.

Figure 4. Observed 24-hour averaged PM₁₀ concentrations and simulated hourly

1000 PM₁₀ concentrations without OBB emissions (No_OBB) and with OBB emissions

based on traditional bottom-up (Traditional_OBB), FRP-based (FRP_OBB) and
constraining (Constrained_OBB) methods in Lianyungang, Fuyang, Bozhou,

1003 Bengbu, Huainan, Hefei, and Chuzhou during June 17-25, 2010.

Figure 5. Observed 24-hour averaged PM₁₀ concentrations and simulated hourly
 PM₁₀ concentrations without OBB emissions (No_OBB) and with OBB emissions
 based on traditional bottom-up (Traditional_OBB), FRP-based (FRP_OBB) and

1007 constraining (Constrained_OBB) methods in Xuzhou, Lianyungang, Fuyang,

1008 Bozhou, Bengbu, Huainan, Hefei, and Chuzhou during June 8-14, 2012.

Figure 6. Annual CO emissions from OBB in YRD obtained in this work and
other studies from 2005 to 2012.

1011 Figure 7. Spatial distributions of CO emissions from OBB obtained in this work

1012 (constraining method), GFAS v1.0, GFED v3.0 and GFED v4.1s in 2010.

- Figure 8. The contribution of OBB to PM₁₀ concentrations for different YRD
 cities during OBB events in June 2010 and 2012.
- Figure 9. The contribution of OBB to PM_{2.5} and PM₁₀ concentrations for
 different YRD cities during OBB event in June 2014.
- 1017 Figure 10. PM₁₀ concentrations contributed by OBB for different YRD cities in
- 1018 Jun 8-14 (PE1) and June 22-28 (PE2), 2012.
- 1019 Figure 11. PM₁₀ concentrations contributed by OBB for different YRD cities
- 1020 based on the diurnal variations of 2010 and 2012 in Jun 8-14, 2010.

TABLES

1023 Table 1. Constrained OBB emissions from 2005 to 2015 in YRD (Unit: Gg).

	PM_{10}	PM _{2.5}	EC	OC	CH_4	NMVOCs	CO	CO_2	NOx	SO_2	NH ₃
2005	175.7	153.7	4.4	38.7	32.1	420.3	670.2	12011.2	22.2	2.7	4.1
2006	171.3	149.9	4.3	37.8	31.3	409.9	653.7	11716.7	21.7	2.6	4.0
2007	219.1	191.7	5.5	48.3	40.0	524.2	835.9	14981.9	27.7	3.4	5.1
2008	176.7	154.6	4.4	39.0	32.3	422.8	674.3	12085.2	22.3	2.7	4.1
2009	178.8	156.4	4.5	39.4	32.6	427.7	682.0	12223.3	22.6	2.8	4.2
2010	257.9	225.7	6.5	58.3	47.6	624.5	987.7	17720.3	33.0	4.0	6.1
2011	188.9	165.3	4.7	41.7	34.5	452.0	720.7	12917.7	23.9	2.9	4.4
2012	389.0	340.4	9.6	83.6	70.2	919.4	1478.6	26473.6	48.6	6.0	9.0
2013	260.7	228.1	6.5	57.5	47.6	623.8	994.7	17828.1	33.0	4.0	6.1
2014	332.4	290.8	8.3	73.3	60.7	795.2	1268.1	22729.0	42.0	5.1	7.8
2015	109.9	96.1	2.8	24.2	20.1	262.9	419.3	7514.6	13.9	1.7	2.6

Table 2. Model performance statistics for concentrations of PM_{2.5} and PM₁₀ from
observation and CMAQ simulation without OBB emissions (No_OBB) and with
OBB emissions based on traditional bottom-up (Traditional_OBB), FRP-based
(FRP_OBB) and constraining methods (Constrained_OBB) for the three OBB
events of June 2010, 2012 and 2014.

			No_	OBB	Tradition	nal_OBB	FRP_	OBB	Constrair	ned_OBB
			NMB	NME	NMB	NME	NMB	NME	NMB	NME
2010	PM_{10}	Daily	-47%	50%	11%	44%	-33%	41%	-16%	37%
2012	PM_{10}	Daily	-60%	68%	-16%	45%	-45%	52%	-10%	45%
	PM ₁₀	Daily	-59%	59%			-54%	54%	-37%	42%
2014		Hourly	-59%	60%			-54%	57%	-37%	52%
2014	DM	Daily	-52%	52%			-41%	42%	-12%	39%
	PM _{2.5}	Hourly	-52%	56%			-41%	51%	-13%	54%
Bench	PM_{10}								-45%	49%
-mark	PM _{2.5}								-33%	43%

1032

1033 Note: ^a from Zhang et al. (2006). NMB and NME were calculated using following equations (*P* 1034 and *O* indicate the results from modeling prediction and observation, respectively):

1035
$$NMB = \frac{\sum_{i=1}^{n} (P_i - O_i)}{\sum_{i=1}^{n} (O_i)} \times 100\%; NME = \frac{\sum_{i=1}^{n} |P_i - O_i|}{\sum_{i=1}^{n} (O_i)} \times 100\%.$$

	PM_{10}	PM _{2.5}	EC	OC	CH_4	NMVOCs	CO	CO_2	NOx	SO_2	NH_3
Traditional (this work)	362.4	317.1	9.3	85.7	67.9	154.9	1391.8	24978.0	47.0	5.4	8.7
FRP-based (this work)	57.8	50.6	6.4	18.5	46.5	412.5	820.1	12718.0	24.9	3.2	17.7
FRP-based (WSE) ¹	158.6	139.1	4.1	38.5	30.1	68.7	612.8	11004.3	20.9	2.4	3.9
Constrained (this work)	257.9	225.7	6.5	58.3	47.6	624.5	987.7	17720.3	33.0	4.0	6.1
GFASv1.0	-	17.8	1.0	9.5	15.6	88.7	196.3	3097.8	5.1	1.0	3.1
GFEDv3.0	-	3.5	0.2	1.7	3.2	4.1	39.4	701.6	1.1	0.2	6.4
GFEDv4.1s	-	33.6	4.0	12.4	31.3	53.2	548.3	8519.7	16.7	2.2	11.7
Xia et al, (2016)	350.2	339.3	14.8	137.8	-	-	1989.9	49835.1	134.3	22.6	-
1											

1037 Table 3. OBB emissions in YRD derived from this work and other studies in
1038 2010 (Unit: Gg).

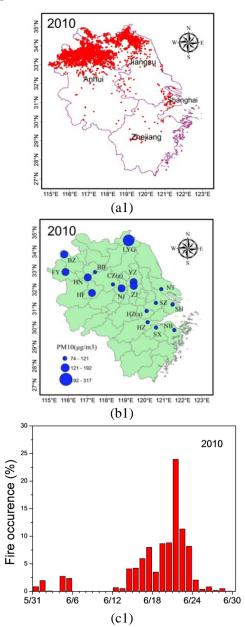
¹ FRP-based (WSE): the OBB emissions were estimated with FRP-based method, applying the same emission factors used in the bottom-up method. The emission factors were obtained

1041 by weighting emission factors in the bottom-up method with the masses of various crop types.

Table 4. The uncertainties of OBB emissions in YRD indicated as 95% CIs and the top two parameters contributing most to emission uncertainties based on traditional bottom-up and FRP-based methods for 2012. The percentages in the parentheses indicate the contributions of the parameters to the variances of emissions.

	Traditior	nal bottom-up method	FRP-base	FRP-based method			
DM	560/ 700/	PCRBF ¹ _{Anhui} (42%)	770/ 2740/	EF (76%)			
PM ₁₀	-56%, +70%	EF_{wheat} (41%)	-77%, +274%	$AF^{2}(11\%)$			
	5604 . 7004	PCRBF _{Anhui} (43%)	(20/	EF (65%)			
PM _{2.5}	-56%, +70%	EF_{wheat} (41%)	-63%, +244%	NFP ³ (16%)			
EC	500/ 540/	PCRBF _{Anhui} (69%)	790/ 0910/	EF (75%)			
EC	-50%, +54%	PCRBF _{Jiangsu} (11%)	-78%, +281%	NFP (11%)			
OC	-54%, +73%	PCRBF _{Anhui} (42%)	-78%, +276%	EF (75%)			
	-34%, +73%	EF_{rice} (37%)	-78%, +270%	NFP (11%)			
CH_4	-49%, +58%	PCRBF _{Anhui} (65%)	-83%, +315%	EF (79%)			
$C\Pi_4$	-+)/0, +30/0	PCRBF _{Jiangsu} (11%)	$-0370, \pm 31370$	NFP (9%)			
NMVOCs	-48%, +59%	PCRBF _{Anhui} (64%)	-63%, +243%	EF (65%)			
INIVI V OCS		PCRBF _{Jiangsu} (10%)	-0370, +24370	NFP (16%)			
СО	-46%, +73%	PCRBF _{Anhui} (62%)	-52%, +223%	EF (57%)			
0		PCRBF _{Jiangsu} (10%)	-5270, 122570	NFP (19%)			
CO_2	-48%, +60%	PCRBF _{Anhui} (69%)	-21%, +164%	NFP (44%)			
	-4070, 10070	PCRBF _{Jiangsu} (10%)	-2170, +10+70	AF (42%)			
NO _X	-47%, +87%	PCRBF _{Anhui} (51%)	-82%, +303%	EF (78%)			
NOX	-4/%,+8/%	$\text{EF}_{wheat}(23\%)$	$-6270, \pm 30570$	NFP (10%)			
SO_2	-59%, +138%	EF_{wheat} (35%)	-78%, +279%	EF (74%)			
502	-39%, +138%	PCRBF _{Anhui} (27%)	-7070, +27970	NFP (12%)			
NH ₃	-51%, +67%	PCRBF _{Anhui} (55%)	-82%, +302%	EF (79%)			
11113	-3170, +07%	EF_{wheat} (12%)	-0270, +302%	NFP (10%)			

¹ PCRBF, the percentage of crop residues burned in the field (the subscript indicates province); ²
 AF, the average FRE of fire pixels; ³ NFP, the number of fire pixels; ⁴ MCRBF, the mass of crop residues burned in the field.



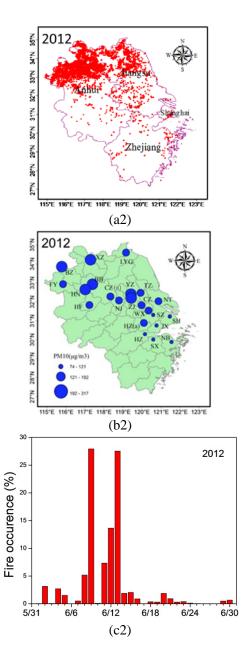




Figure 2.

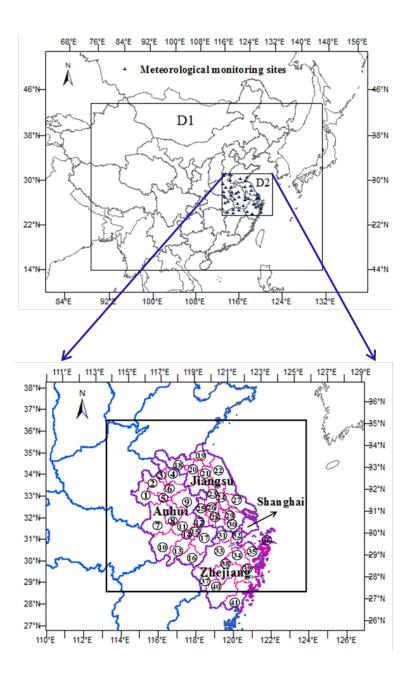
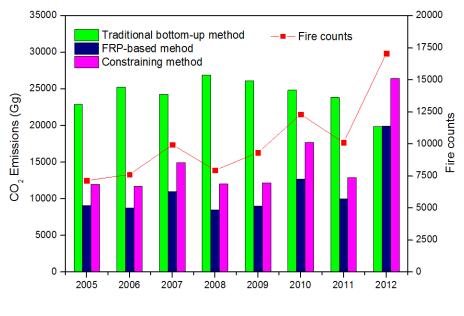
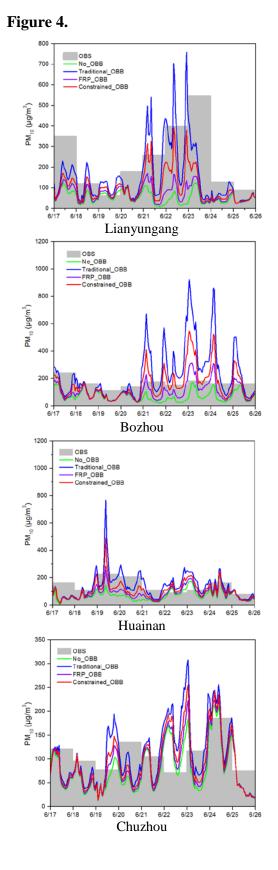
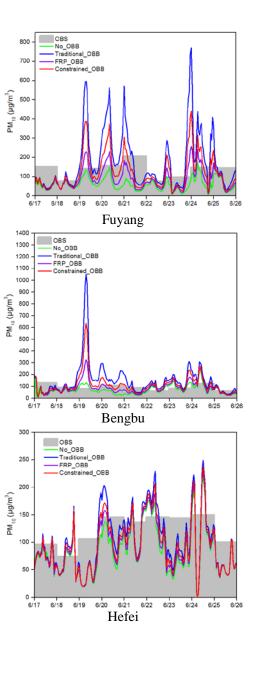


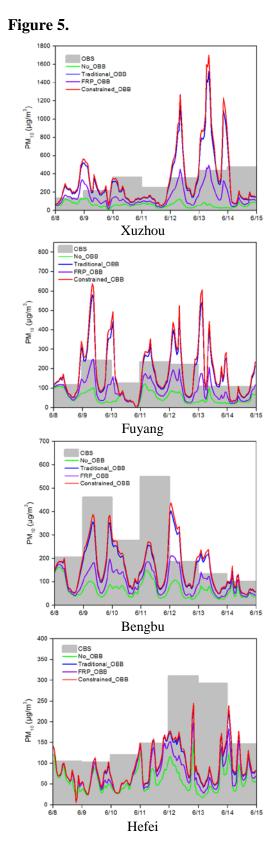


Figure 3.









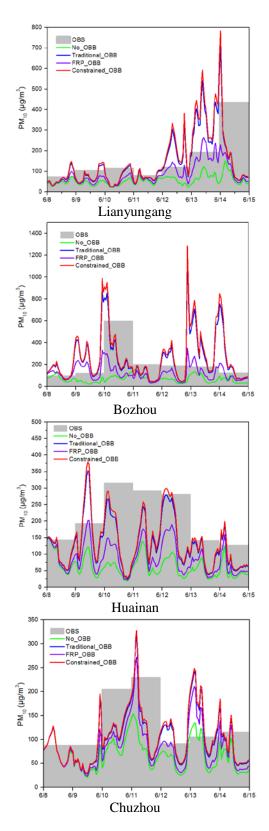
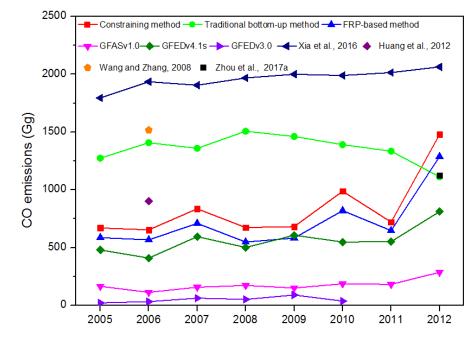




Figure 6.





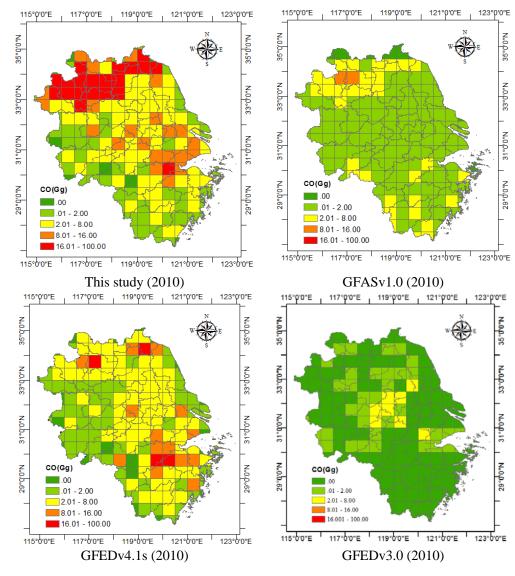




Figure 8.

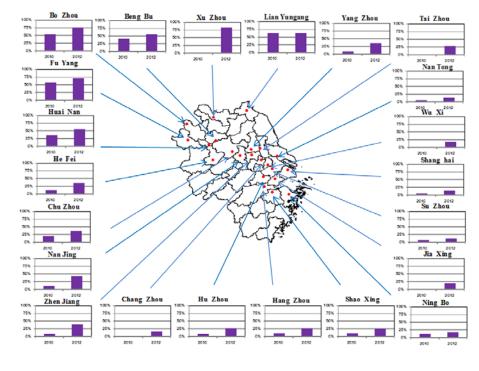


Figure 9.

